Nanoscale Advances

PAPER

View Article Online
View Journal | View Issue

Cite this: *Nanoscale Adv.*, 2019, **1**, 3680

$Ti_{n+1}C_n$ MXenes with fully saturated and thermally stable Cl terminations†

J. Lu,[a] I. Persson,[a] H. Lind,[a] J. Palisaitis,[a] M. Li,[b] Y. Li,[b] K. Chen,[b] J. Zhou,[ab] S. Du,[b] Z. Chai,[b] Z. Huang,[b] L. Hultman,[a] P. Eklund,[a] J. Rosen,[a] Q. Huang[b] and P. O. Å. Persson*[a]

Received 23rd May 2019
Accepted 8th July 2019

DOI: 10.1039/c9na00324j

rsc.li/nanoscale-advances

MXenes are a rapidly growing family of 2D materials that exhibit a highly versatile structure and composition, allowing for significant tuning of the materials properties. These properties are, however, ultimately limited by the surface terminations, which are typically a mixture of species, including F and O that are inherent to the MXene processing. Other and robust terminations are lacking. Here, we apply high-resolution scanning transmission electron microscopy (STEM), corresponding image simulations and first-principles calculations to investigate the surface terminations on MXenes synthesized from MAX phases through Lewis acidic melts. The results show that atomic Cl terminates the synthesized MXenes, with mere residual presence of other termination species. Furthermore, *in situ* STEM-electron energy loss spectroscopy (EELS) heating experiments show that the Cl terminations are stable up to 750 °C. Thus, we present an attractive new termination that widely expands the MXenes' functionalization space and enables new applications.

Introduction

MXenes constitute a rapidly growing addition[1,2] to the family of 2D materials with excellent properties and performance in terms of electrochemical charge storage,[3,4] electromagnetic interference shielding,[5] filtering,[6] and more recently also carbon capture,[7] in addition to a range of other applications.[8,9] MXenes are predominantly obtained from the parent inherently nanolaminated $M_{n+1}AX_n$ (MAX) phases where M is a transition metal, A is a group A element (mostly group 13 and 14) and X is C and/or N.[10] By chemical etching of the atomically thin A element layers that interleave sheets of $M_{n+1}X_n$, these sheets are separated from each other and their surfaces are immediately functionalized by surface terminating species, T_x,[11,12] that typically originate from the etchant. Accordingly, $M_{n+1}X_nT_x$ most appropriately describe MXenes. From this formula, it is apparent that the MXene properties can be tuned through variations in structure, composition, and surface terminations. The structure is inherited from the parent MAX phase (hexagonal, space group $P6_3/mmc$), but compositional tuning displays an extraordinary toolbox for property tuning. This can be achieved through MXenes based on single M and X elements, as well as with alloys on both M and X.[2,13] In addition, there are reports on MXenes forming out-of-plane[14] and in-plane[15] double-M elemental ordering, as well as vacancy-ordered structures.[16,17]

Manipulation of the surface terminations constitutes the final and arguably the most important variable for property tuning,[18] yet it is the experimentally least explored. Currently, the MXene preparation dictates that T_x is inherent to the etchant and thus predominantly a combination of O and F, whose ratio can be tailored,[19] where also OH has been considered as a minor[20] or even negligible contribution.[21] Despite several theoretical investigations considering single,[18,22] mixed,[23,24] and non-inherent[25–27] termination species, particularly the non-inherent terminations have remained relatively unexplored experimentally. Persson *et al.* explored a route for removing the inherent surface terminations through a combination of heating and H_2 etching, while also re-terminating the MXene surface from the gas phase with non-inherent species (*e.g.* CO_2).[7] However, to further expand the already vast property space of MXenes, non-traditional synthesis routes and new terminations must be considered.

In the present communication, we report on MXenes that are exclusively Cl-terminated by synthesis from MAX phases through Lewis acidic melts. Through this approach, the MAX phase A elements are replaced by late transition-metal halides, in this case Zn, which is subsequently exfoliated and the emerging MXene sheets are Cl terminated.[28] These results are significant, not only because they demonstrate Cl as an exclusive surface-terminating species for MXenes, but also because the Cl terminations are highly stable, and thus offer a novel avenue for tailoring the properties of MXenes.

[a]*Thin Film Physics Division, Department of Physics, Chemistry and Biology (IFM), Linköping University, SE-581 83 Linköping, Sweden. E-mail: per.persson@liu.se*
[b]*Engineering Laboratory of Advanced Energy Materials (FiNE Lab.), Ningbo Institute of Industrial Technology, Chinese Academy of Sciences, Ningbo, Zhejiang, 315201, China*

† Electronic supplementary information (ESI) available. See DOI: 10.1039/c9na00324j

Experiments

As described in a complementary paper,[28] MXene powder samples were synthesized by mixing homemade MAX phase powders, containing both Ti_2AlC and Ti_3AlC_2, with $ZnCl_2$ at a 1 : 1.6 molar ratio and heating at 550 °C for 5 h. The resulting bulk product was crushed into powder and cleansed with aqueous HCl at ambient temperature. Then, the reacted material was obtained and purified with deionized water. The final powder sample was analyzed by scanning electron microscopy (SEM), X-ray diffraction (XRD) and X-ray photoelectron spectroscopy (XPS) to obtain the microstructural and chemical composition and the yield of the obtained material. For detailed information on the preparation process, please see ref. 28.

The atomic structural and chemical analyses were carried out by high-resolution high angle annular dark field scanning transmission electron microscopy (HAADF-STEM) imaging and lattice resolved energy dispersive X-ray (EDX) spectroscopy using a Linköping double Cs corrected FEI Titan^3 60-300 microscope, operated at 300 kV and equipped with a high sensitivity Super-X EDX detector. The corresponding HAADF-STEM images were simulated using Dr. Probe software for imaging conditions with high accuracy matching the experimental setup. Supercells of Ti_2CCl_2 and $Ti_3C_2Cl_2$ were constructed employing CrystalMaker with lattice parameters obtained from DFT calculations reported in the present paper.[29] Compositions of the structures were obtained using the built-in functions of ESPRIT software.

In situ heating of the samples was carried out using a furnace type heating holder (Gatan Model 652). The heating rate was approximately 200 °C per min in steps of 50 °C and each temperature was kept for 30 minutes. EELS spectra were continuously acquired during heating using a Gatan Quantum ERS GIF. The resulting spectra were processed by background subtraction and plural scattering deconvolution routines embedded in Digital Micrograph software.

Our calculations were carried out on primitive cells of Cl-terminated Ti_2C and Ti_3C_2. A total supercell height of 40 Å was used to avoid self-interaction between MXene sheets across the periodic boundaries. We carried out first-principles calculations of total energies, density of states and band structures using Density Functional Theory (DFT) with plane wave methods as implemented in Vienna *Ab initio* Simulation Package (VASP) software.[30,31] The exchange–correlation effects were treated within the generalized gradient approximation (GGA) of Perdew–Burke–Ernzerhof (PBE).[32] The cutoff energy for the plane-wave expansion was set to 400 eV, which is equal to that recommended for the VASP potentials used, and provides adequate precision for our purposes. A 25 × 25 × 1 mesh of *k*-points was used during structural relaxation of 1 × 1 Ti_3C_2 and Ti_2C. Self-consistency criteria were set to 2×10^{-5} eV f.u.$^{-1}$ on electronic convergence and 5×10^{-5} eV f.u.$^{-1}$ on forces. Such relaxations were carried out on multiple lattice parameters (in-plane *a*) to determine the equilibrium size, the results of which were fitted to a Morse type equation of state.[33] Once an equilibrium lattice parameter was determined, accurate density of states and band structures were calculated using larger meshes of 29 × 29 × 1 for DOS, while the band structure was calculated at 120 points between each pair of high symmetry points, and self-consistency was within 10^{-5} eV f.u.$^{-1}$ Cl_2 molecules were calculated as well by placing the molecule in a box 20 Å in size, with self-consistency being within 10^{-5} eV per molecule. We determined its bond length to be 1.9928 Å, which corresponds well with the experimentally expected value of 1.99 Å.

Results

Fig. 1(a) shows the atomically resolved structure of a thin edge from a larger multilayer particle. In the thinnest areas, the structure exhibits the characteristic honeycomb appearance of a single sheet of a 2-dimensional M_2XT_x MXene, where bright dots correspond to the M element (Ti). The X element (carbon) is positioned in the core of the honeycomb, but is barely visible due to the mass contrast experimental conditions (intensity ~ Z^2). Electron diffraction patterns obtained from the same particle further confirm a hexagonal structure (see Fig. S1†). An overview image of a multilayer particle and the corresponding EDX elemental maps for Ti and Cl are shown in Fig. 1(b)–(d), respectively. Residual O was found in the EDX spectra, predominantly originating from the bright rectangular features on the surfaces of the multilayer particle, but with no contribution from other elements. The EDX maps demonstrate that Ti and Cl are present in the multilayer particles, while the EDX spectrum additionally identifies C in addition to the O

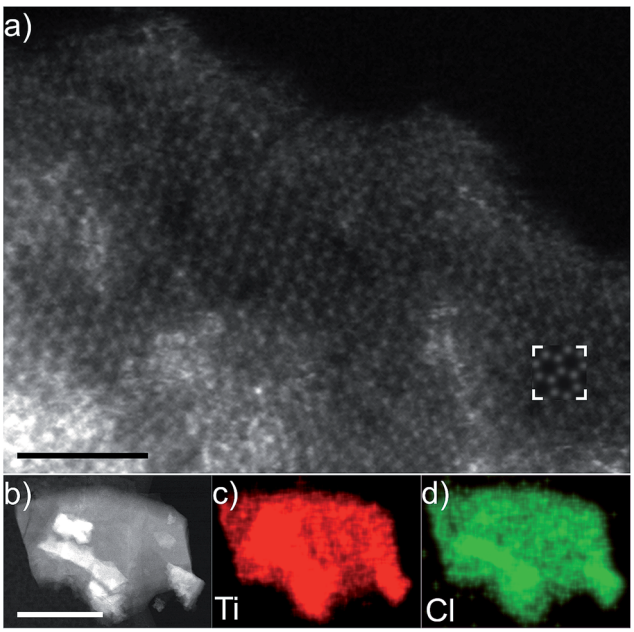

Fig. 1 (a) Atomically resolved plan-view HAADF-STEM image of a Ti_2CT_x MXene multilayer particle and (b) a low magnification overview with corresponding (c) Ti and (d) Cl elemental maps. Note that the inset in (a) is showing a simulated plan-view STEM image of Ti_2CCl_2 (middle right). The scale bar in (a) corresponds to 2 nm and in (b) it corresponds to 0.5 μm.

originating from the rectangular features (local EELS spectra at the particle edges reveal an O contribution in line with the noise level – not shown). This indicates that Cl is present as a surface termination on the Ti_3C_2 MXene. The location of the Cl termination can be inferred from the high resolution image shown in Fig. 1(a). Given that little or no contrast originates from the plan view observed honeycomb core, there is no terminating atom present on that site. The honeycomb core corresponds to the hcp site, which then indirectly identifies the fcc site as the preferred site for Cl terminations (see the ESI, Fig. S2†, for a schematic description of the fcc/hcp sites). A STEM image simulation of a Cl-terminated Ti_2C single sheet, with the terminations residing on the fcc site, is shown in the inset in Fig. 1(a) (middle right). The simulation shows that the atomic columns (bright dots corresponding to Ti + Cl atoms in the plan view) exhibit a homogeneous contrast, which matches the STEM image qualitatively.

Additional cross-sectional structural characterization was performed for similar particles as shown in Fig. 2. The figure shows the layered characteristics of terminated Ti_2C (Fig. 2(a) and (c)) and Ti_3C_2 (Fig. 2(b) and (d)) MXenes from [11−20] and [1−100] orientations, respectively. The STEM images show that the sample consists of stacked MXene sheets, each exhibiting bright atomic columns in the middle of the sheet and two darker surface layers. The images reveal that the layers are closely stacked, yet it is apparent that there is local bending, from which weak attraction between the layers can be inferred. Presumably, intercalation by DMSO and sonication would entirely separate the sheets as in previous investigations of MXene multilayers.

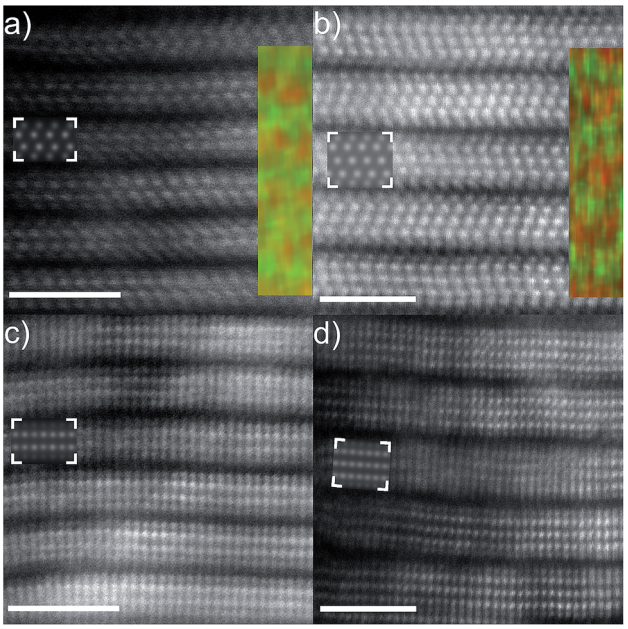

Fig. 2 Atomically resolved cross-sectional HAADF-STEM images for {11−20} oriented (a) Ti_2CCl_2 and (b) $Ti_3C_2Cl_2$, and for {1−100} oriented (c) Ti_2CCl_2 and (d) $Ti_3C_2Cl_2$. The colored insets in (a) and (b) correspond to lattice resolved EDX elemental maps showing Ti (red) and Cl (green). Note that the insets are showing simulated cross-sectional STEM images of Ti_2CCl_2 and $Ti_3C_2Cl_2$ for each orientation. Scale bars correspond to 2 nm.

According to the inserted lattice resolved EDX elemental maps and by overlaying Ti (red) and Cl (green) it is clear that the darker surface terminations consist of Cl, as seen from both the M_2X and M_3X_2 structures. Residual amounts of O were also observed during cross-sectional mapping, presumably originating from exposure to ambient conditions during sample transfer and handling. According to the EDX measurements, the Ti : Cl ratio is very close to 2 : 2 and 3 : 2, which directly corresponds to the observed number of layers and indicates exclusively Cl-terminated Ti_3C_2 and Ti_2C MXenes (see Fig. S3† for direct illustration of the relative Ti : Cl ratios).

It is worth noting that the surface terminations are highly ordered, *e.g.* seemingly acceptable equilibrium lattice positions. In previous observations of O- and F-terminated MXenes,[21] it was found that the terminations exhibit a significant degree of disorder on materials prepared under ambient conditions. Here, the material was prepared during a high-temperature process, using temperatures equivalent to those in previous *in situ* observations of ordering among terminations,[21] which explains the highly ordered appearance.

The high degree of order among the surface terminations enables exact determination of the preferred site on the MXene surface. Combining the complementary information available from the [11−20] and [1−100] orientations, it is clear that Cl preferentially occupies the fcc site, in agreement with theoretical predictions.[34] This is further confirmed by the HAADF-STEM image simulations with Cl on the fcc site, which are overlaid as insets in Fig. 2(a)–(d) where the simulated intensities qualitatively match the experimentally observed intensity difference between Ti and Cl layers.

However, from the STEM images above, it is also clear that the layer of Cl terminations is significantly separated from the nearest Ti layer, approximately 1.71 Å as measured for Ti_2C from Fig. 2(c) and 1.84 Å for Ti_3C_2 from Fig. 2(b). This translates to a Ti–Cl bond length of 2.45 and 2.55 Å for an *a* lattice parameter of 3.05 Å in Ti_2C and Ti_3C_2, respectively, which is typically much more than for other terminations. Previous experiments yield a Ti–O/F bond length of 2.11 Å for pristine Ti_3C_2 (translating to a Ti–O/F layer separation of 1.23 Å).[35]

Finally, the individual Cl-terminated MXene sheets are mutually translated along the basal plane compared to, *e.g.*, O-terminated MXenes, where the fcc sites of two adjacent layers are located directly on top of each other, see Fig. 2(b).

DFT calculations were performed for Cl-terminated Ti_2C and Ti_3C_2, and it was found that Cl terminations prefer fcc sites over hcp or mixed for both structures in agreement with the experimental findings and previous calculations (see Fig. S4† for further information). Moreover, and in excellent agreement with the STEM images, the interplanar distance between the Cl terminations and the first Ti layer is exceptional and corresponds to 1.67 and 1.70 Å for Ti_2C and Ti_3C_2, which corresponds to a calculated Ti–Cl bond length of 2.51 Å for both Ti_2C and Ti_3C_2. In comparison, the Ti–C planes are separated by 1.09 and 1.03 Å (Ti_2C and Ti_3C_2-nearest surface). See Table S1† for calculated spacings.

Fig. 3 shows the electronic structure, including the band structure and projected density of states, determined using the fully relaxed structures of the MXenes, with Cl terminations in the fcc sites. For both Ti_2C and Ti_3C_2, the DOS and band structures are very similar, both showing well defined metallicity with the Fermi level dominated by Ti d-orbitals. In addition, there are strong indicators of hybridization between Ti d-, and C p- and Cl p-orbitals in the energy range between −2 and −7 eV. The difference between Ti_2C and Ti_3C_2 is mainly that there are more Ti and C bands in the Ti_3C_2 case. There is also a small gap in the band structure around −2 eV for Ti_2C, whereas in Ti_3C_2 that gap is closed.

Furthermore, the formation energy, E_{form}, of bonded Cl atoms on the surface was determined, as defined by the following formula:

$$E_{form} = E(Ti_{n+1}C_nT_2) - E(Ti_{n+1}C_n) - E(T_2)$$

here, $E(Ti_{n+1}C_nT_2)$ refers to energy of the MXene surface with terminations T, while $E(Ti_{n+1}C_n)$ is the energy of the non-terminated surface, and $E(T_2)$ is the energy of a free molecule of the terminations (here Cl_2). According to this, the formation energy becomes −6.901 eV per formula unit (f.u.) for Ti_2CCl_2, while the formation energy for $Ti_3C_2Cl_2$ is −6.694 eV f.u.$^{-1}$. This can be compared to the formation energies of O-terminated $Ti_3C_2O_2$ and N-terminated $Ti_3C_2N_2$, which are −9.656 and −2.596 eV f.u.$^{-1}$, respectively, as shown in our previous article.[21] While not as stable as O, the Cl terminations can be expected to bond strongly to the MXene surfaces.

To investigate whether the relaxed structure was dynamically stable with respect to lattice vibrations, the phonon dispersion relations were calculated for both $Ti_3C_2Cl_2$ and Ti_2CCl_2 with Cl terminations in both fcc and hcp sites. As can be seen from Fig. S5,† all phonon branches are real, indicating that Cl constitutes a stable termination, regardless of coordination.

To experimentally investigate the calculated high stability of Cl terminations, the $Ti_3C_2Cl_2$ and the Ti_2CCl_2 powders were heated *in situ* up to 800 °C in the (S)TEM. The structural and elemental changes during heating were followed by (S)TEM imaging and electron energy loss spectroscopy (EELS). Fig. 4 shows the background-subtracted and plural-scattering-deconvolved EEL spectra from a $Ti_3C_2Cl_2$ particle as a variation of temperature. The spectra show the Cl-$L_{3,2}$ and Ti-$L_{3,2}$ edges at ∼200 and ∼450 eV energy loss, respectively, and are normalized against the Ti-L edge since the number of M layers does not change during heating. The EELS measurements additionally detected both carbon and oxygen, where additional carbon appears with temperature, presumably through beam induced contamination during the measurements, and where the O is present (∼5%) from the initial measurement and remains stable. Notably, the extended fine structure of the Cl-$L_{3,2}$ edge indicates that Cl is present as a compound component, in agreement with the XPS results[28] which identified a Ti–Cl bond in the emerging MXene powder. Together, XPS on the macroscopic scale and the EELS on the microscopic scale identify Cl as an MXene termination.

The results show that $Ti_3C_2Cl_2$ is stable at temperatures below ∼750 °C. At this temperature and above, the MXene

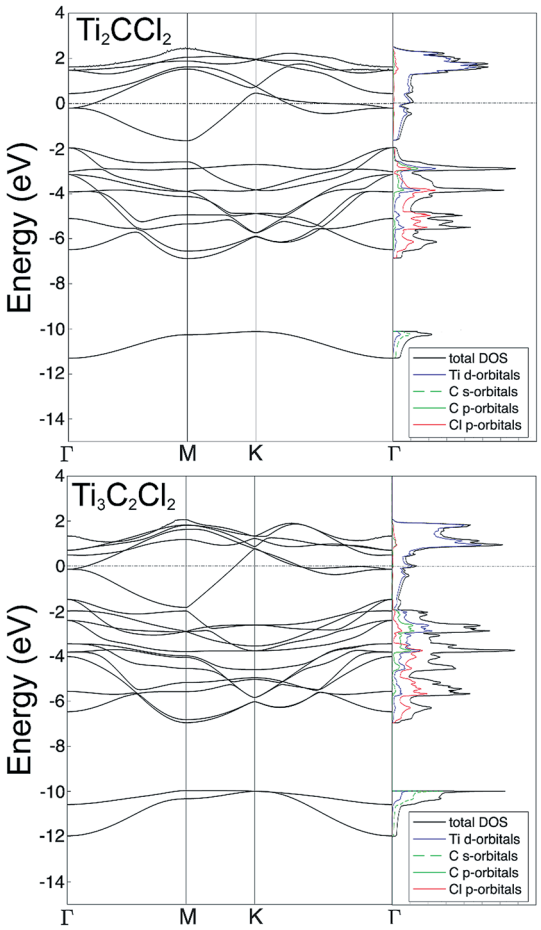

Fig. 3 Band structure and electronic density of states, resulting from the DFT calculations, for Ti_2C (top) and Ti_3C_2 (bottom) with fcc coordinated Cl terminating the MXene surfaces.

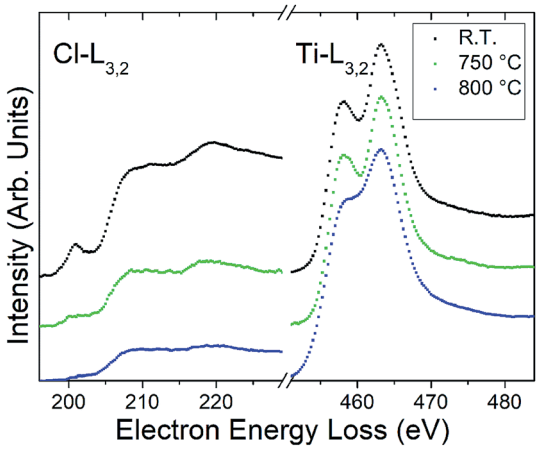

Fig. 4 Electron energy loss spectroscopy from a thin edge of a $Ti_3C_2T_2$ multilayer particle, showing the background subtracted and multiple scattering deconvolved Cl- and Ti-$L_{3,2}$ edges under ambient conditions and after heating at 750 and 800 °C. The spectra are normalized against the Ti-L_2 peak maximum and vertically separated for clarity.

gradually decomposes together with an apparent loss of Cl terminations. The loss is stronger at the thin edges of the MXene multilayer particle compared with the "bulk" of the particle, which is presumably due to a slow Cl diffusion–desorption process. After heating at 800 °C, residual Cl remains in the multilayer particle. The loss of surface terminations from MXenes during heating has been observed also for F, which desorbs at similar temperatures to Cl, but not for O which remains stable on the surface.[21] The high stability calculated for Cl terminations is therefore in agreement with the experimental findings. Note that the fine structure of the Ti-$L_{3,2}$ edge becomes smeared at the highest temperature which is presumably due to an increasing disorder among the remaining surface terminations and in the microstructure. The microstructure of the MXene sheets is indeed subject to degradation. While the laminated structure is preserved, an increasing amount of black spots appear, particularly apparent in the thinnest regions (see Fig. S4†). These spots are interpreted as nanoscale voids, presumably formed by a local mechanical deformation of the MXene structure as Cl gas forms from the desorbing terminations.

Discussion and conclusions

Cl has been investigated as a terminating species on Ti_3C_2 and Ti_2C MXenes. From high resolution (S)TEM imaging and lattice resolved EDX mapping, Cl was found to occupy the fcc sites of the MXene surface. Furthermore, the EELS results reveal that Cl is present on the surfaces in a compound state as opposed to a molecular state, which indicate that the CL is bound to the MXene surface. In contrast to most etched MXenes, the surface terminations assume a highly ordered appearance even at ambient temperatures, which is attained through the preceding high temperature processing.

A mix of terminations, such as Cl, O and F, has been reported previously, where the MXene was etched from MAX powders using aqueous LiF–HCl[36] or aqueous HCl,[37] enforcing the mixing of terminations. These termination-mixed MXenes resulted in an improved electrochemical rate capability, which was explained by an observed increase in interlayer spacing, causing improved ion accessibility. The present results provide further support for this explanation. The very large separation observed here between the layer of Cl terminations and the underlying Ti surface is suggested to cause local undulations in a mixed termination layer which increases the average interlayer spacing. Theoretical calculations have predicted an exclusively Cl-terminated Ti_2C MXene to exhibit a very large voltage window (3.5–4 V),[34] which pinpoints the importance of further investigating routes for tailoring the MXene surface terminations.

In situ TEM heating further shows that the Cl terminations are thermally stable below 750 °C, above which point they increasingly desorb, presumably as Cl gas, while the MXene structure additionally degrades through the formation of local nanoscale voids. After heating at 800 °C only residual Cl remains on the surface.

The present results identify MXenes that are exclusively terminated by Cl. These were formed by MXene synthesis using Lewis acidic melts to extract the A-layer at high temperatures. This method shows promise as a feasible way to synthesize new MXenes with single-component surface terminations. Consequently, the present communication extends the range of available surface chemistries on MXenes and facilitates tailoring of the amount of Cl terminations, from mixed (O + F + Cl and O + Cl) to exclusively Cl-terminated. Moreover, these findings stress that MXene terminations are not limited to F and O and that new and more terminations remain to be identified.

Conflicts of interest

There are no conflicts to declare.

Acknowledgements

The authors acknowledge the Swedish Research Council for funding under Grant No. 2016-04412 and 2013-8020, the Swedish Government Strategic Research Area in Materials Science on Functional Materials at Linköping University (Faculty Grant SFO-Mat-LiU No. 2009 00971), and the National Natural Science Foundation of China (Grant No. 21671195 and 91426304). The Knut and Alice Wallenberg Foundation is acknowledged for support of the electron microscopy laboratory in Linköping, fellowship grants and a project grant (KAW 2015.0043). P. O. Å. P. and J. R. also acknowledge the Swedish Foundation for Strategic Research (SSF) for project funding (EM16-0004) and the Research Infrastructure Fellow RIF 14-0074.

References

1 M. Naguib, M. Kurtoglu, V. Presser, J. Lu, J. J. Niu, M. Heon, L. Hultman, Y. Gogotsi and M. W. Barsoum, *Adv. Mater.*, 2011, **23**, 4248.
2 M. Naguib, O. Mashtalir, J. Carle, V. Presser, J. Lu, L. Hultman, Y. Gogotsi and M. W. Barsoum, *ACS Nano*, 2012, **6**, 1322.
3 M. Ghidiu, M. R. Lukatskaya, M.-Q. Zhao, Y. Gogotsi and M. W. Barsoum, *Nature*, 2014, **516**, 78.
4 B. Anasori, M. R. Lukatskaya and Y. Gogotsi, *Nat. Rev. Mater.*, 2017, **2**, 16098.
5 F. Shahzad, M. Alhabeb, C. B. Hatter, B. Anasori, S. Man Hong, C. M. Koo and Y. Gogotsi, *Science*, 2016, **353**, 1137.
6 Q. Peng, J. Guo, Q. Zhang, J. Xiang, B. Liu, A. Zhou, R. Liu and Y. Tian, *J. Am. Chem. Soc.*, 2014, **136**, 4113.
7 I. Persson, J. Halim, H. Lind, T. W. Hansen, J. B. Wagner, L.-Å. Näslund, V. Darakchieva, J. Palisaitis, J. Rosen and P. O. Å. Persson, *Adv. Mater.*, 2018, 1805472.
8 V. M. H. Ng, H. Huang, K. Zhou, P. S. Lee, W. Que, J. Z. Xu and L. B. Kong, *J. Mater. Chem. A*, 2017, **5**, 3039.
9 P. Eklund, J. Rosén and P. O. Å. Persson, *J. Phys. D: Appl. Phys.*, 2017, **50**, 113001.
10 M. W. Barsoum, *Prog. Solid State Chem.*, 2000, **28**, 201.
11 M. Naguib, V. N. Mochalin, M. W. Barsoum and Y. Gogotsi, *Adv. Mater.*, 2014, **26**, 992.

12 P. Srivastava, A. Mishra, H. Mizuseki, K.-R. Lee and A. K. Singh, *ACS Appl. Mater. Interfaces*, 2016, **8**, 24256.
13 M. Naguib, J. Halim, J. Lu, L. Hultman, Y. Gogotsi and M. W. Barsoum, *J. Am. Chem. Soc.*, 2013, **135**, 15966.
14 B. Anasori, Y. Xie, M. Beidaghi, J. Lu, B. C. Hosler, L. Hultman, P. R. C. Kent, Y. Gogotsi and M. W. Barsoum, *ACS Nano*, 2015, **9**, 9507.
15 I. Persson, A. el Ghazaly, Q. Tao, J. Halim, S. Kota, V. Darakchieva, J. Palisaitis, M. W. Barsoum, J. Rosen and P. O. Å. Persson, *Small*, 2018, **4**, 1703676.
16 Q. Tao, M. Dahlqvist, J. Lu, S. Kota, R. Meshkian, J. Halim, J. Palisaitis, L. Hultman, M. W. Barsoum, P. O. Å. Persson and J. Rosen, *Nat. Commun.*, 2017, **8**, 14949.
17 R. Meshkian, M. Dahlqvist, J. Lu, B. Wickman, J. Halim, J. Thörnberg, Q. Tao, S. Li, S. Intikhab, J. Snyder, M. W. Barsoum, M. Yildizhan, J. Palisaitis, L. Hultman, P. O. Å. Persson and J. Rosen, *Adv. Mater.*, 2018, **30**, 1706409.
18 M. Khazaei, A. Ranjbar, M. Arai, T. Sasaki and S. Yunoki, *J. Mater. Chem. C*, 2017, **5**, 2488.
19 Y. Dall'Agnese, M. R. Lukatskaya, K. M. Cook, P.-L. Taberna, Y. Gogotsi and P. Simon, *Electrochem. Commun.*, 2014, **48**, 118.
20 M. A. Hope, A. C. Forse, K. J. Griffith, M. R. Lukatskaya, M. Ghidiu, Y. Gogotsi and C. P. Grey, *Phys. Chem. Chem. Phys.*, 2016, **18**, 5099.
21 I. Persson, L.-Å. Näslund, J. Halim, M. W. Barsoum, J. Palisaitis, V. Darakchieva, J. Rosen and P. O. Å. Persson, *2D Materials*, 2017, **5**, 015002.
22 Q. Tang, Z. Zhou and P. Shen, *J. Am. Chem. Soc.*, 2012, **134**, 16909.
23 T. Hu, M. Hu, B. Gao, W. Li and X. Wang, *J. Phys. Chem. C*, 2018, **122**, 18501.
24 N. M. Caffrey, *Nanoscale*, 2018, **10**, 13520.
25 A. N. Enyashin and A. L. Ivanovskii, *J. Phys. Chem. C*, 2013, **117**, 13637.
26 N. Li, X. Chen, W. -J. Ong, D. R. MacFarlane, X. Zhao, A. K. Cheetham and C. Sun, *ACS Nano*, 2017, **11**, 10825.
27 Y. Shao, F. Zhang, X. Shi and H. Pan, *Phys. Chem. Chem. Phys.*, 2017, **19**, 28710.
28 M. Li, K. Luo, Y. Li, J. Lu, K. Chang, K. Chen, J. Zhou, J. Rosen, P. Eklund, P. O. Å. Persson, S. Du, Z. Chai, Z. Huang and Q. Huang, *J. Am. Chem. Soc.*, 2019, **141**, 114730–114737.
29 J. Barthel, *Ultramicroscopy*, 2018, **193**, 1–11.
30 G. Kresse and J. Hafner, *Phys. Rev. B: Condens. Matter Mater. Phys.*, 1994, **49**, 14251.
31 G. Kresse and J. Furthmüller, *Phys. Rev. B: Condens. Matter Mater. Phys.*, 1996, **54**, 11169.
32 J. P. Perdew, K. Burke and M. Ernzerhof, *Phys. Rev. Lett.*, 1996, **77**, 3865.
33 V. Moruzzi, J. Janak and K. Schwarz, *Phys. Rev. B: Condens. Matter Mater. Phys.*, 1988, **37**, 790.
34 D. Wang, Y. Gao, Y. Liu, Y. Gogotsi, X. Meng, G. Chen and Y. Wei, *J. Mater. Chem. A*, 2017, **5**, 24720.
35 C. Shi, M. Beidaghi, M. Naguib, O. Mashtalir, Y. Gogotsi and S. J. L. Billinge, *Phys. Rev. Lett.*, 2014, **112**, 125501.
36 S. Kajiyama, L. Szabova, H. Iinuma, A. Sugahara, K. Gotoh, K. Sodeyama, Y. Tateyama, M. Okubo and A. Yamada, *Adv. Energy Mater.*, 2017, **7**, 1601873.
37 W. Sun, S. A. Shah, Y. Chen, Z. Tan, H. Gao, T. Habib, M. Radovic and M. J. Green, *J. Mater. Chem. A*, 2017, **5**, 21663.